Photocopy and Use Authorization

In presenting this thesis in partial fulfillment of the requirements for an advanced degree at Idaho State University, I agree that the Library shall make it freely available for inspection. I further state that permission for extensive copying of my thesis for scholarly purpose may be granted by the Dean of the Graduate School, Dean of my academic division, or by the University Librarian. It is understood that any copying or publication of this thesis for financial gain shall not be allowed without my written permission.

Signature ____________________________________

Date ____

Mapping of Human Hand Actions Using Motion Capture for Dexterous Robotic Telemanipulation

by

Mohammed Shaifur Rahman Chowdhury

A thesis

Submitted in partial fulfillment

of the requirements for the degree of

Master of Science in Mechanical Engineering

Idaho State University

Spring 2018

Committee Approval

To the Graduate Faculty:

The members of the committee appointed to examine the thesis of MOHAMMED SHAIFUR RAHMAN CHOWDHURY find it satisfactory and recommend that it be accepted.

Dr. Alba Perez

Major Advisor

Dr. Marco Schoen

Committee Member

Nancy Devine

Graduate Faculty Representative

Acknowledgements

I would like to express my sincere gratitude to my advisor Dr. Alba Perez for her continuous support, motivation and cooperation. Without her guidance and support my thesis work would have been very difficult. I would like to thank Dr. Marco Schoen for his help and guidance during my Masters study and Nancy Devine to be my Graduate Faculty Representative.

I would also like to thank my classmates at ISU, whose help and companionship was always a great source of inspiration for me.

Special thanks to my parents, elder brother and my wife. Without their continuous supports it would be difficult for me to accomplish my goal.

TABLE OF CONTENTS

List of Figures	VII
List of Tables	IX
Abstract	X
1. Introduction	1
1.1. Thesis Goal	1
1.2. Literature Review	2
1.3. Organization of the thesis	4
2. Mathematical Background	5
2.1. Three-dimensional Space	5
2.2. Kinematics and Rigid Body	6
2.3. Translation	7
2.4. Rotation	7
2.5. General Motion	9
2.6. Composition of Displacements	10
2.7. Least Square Plane Fit and Normal of a Plane	10
2.8. Projection of a Point onto a Plane	13
2.9. The Denavit-Hartenberg Convention	14
2.10. Forward Kinematics	15
2.11. Forward kinematics of Barrett Hand	15

2.11.1. Forward Kinematics of Finger 1 17

2.11.2. Forward Kinematics of Finger 3 18

3. Experimental Setup 21

3.1. Vicon Motion Capture System 21

3.2. Data Collection 23

3.2.1. Marker Placement 23

3.2.2. Motion Capture 25

4. Mapping 29

4.1. 3D Motions to Planer Motions 29

4.2. Mapping to Barrett Hand BH282 36

5. Results 43

6. Conclusion and Future Work 45

References 46

List of Figures

Figure 2.1: Three-dimensional cartesian space	5
Figure 2.2: Motion of a rigid body	6
Figure 2.3: (a) translation, (b) rotation	9
Figure 2.4: Least square fit of a plane from set of n points	12
Figure 2.5: Projection of a point onto a plane	13
Figure 2.6: Local transformation along the links of a robot	15
Figure 2.7: Cross-section of Barrett Hand	16
Figure 2.8: DH frame for Finger 1	17
Figure 2.9: DH frame for Finger 3	19
Figure 3.1: A camera of Vicon Nexus® system	21
Figure 3.2: Vicon motion capture system (camera setup)	22
Figure 3.3: Positions of markers on fingers	23
Figure 3.4: Subject performing grasping task	24
Figure 3.5: Frame of motion	25
Figure 3.6: Snap of the motion capture data	26
Figure 3.7: (a) grasp & raise, (b) grasp & leave, (c) grasp & push motion	28
Figure 4.1: plane for 1^{st} frame of data	31
Figure 4.2: Projected points for 1^{st} frame comparing to the originals	32
Figure 4.3: Mapped motion of the human hand	35

Figure 4.4: Mapped motion of the human hand 35

Figure 4.5: Motions of lt_1 and lp_1 39

Figure 5.1: expected and achieved trajectories of the motion of the robot fingers 43

Figure 5.2: Finger 1 and 3 positions and joint angles for 8 positions 44

List of Tables

Table 2.1: Denavit-Hartenberg parameters 14

Table 2.2: DH parameter values 16

Table 2.3: DH link parameters of Finger 1 17

Table 2.4: DH link parameters of Finger 3 19

Table 4.1: Position of the markers in 1st frame 30

Table 4.2: Values of xo, yo and θ 42

Abstract

The objective of this thesis is the kinematic mapping of human hand motion for dexterous telemanipulation. Different tasks and grasps are considered for human hand motion. The human hand motions are captured by Vicon Motion Capture System which allows an accurate detection of the human hand motion in Cartesian space. In this study, for grasping motion, only the thumb and index finger of the right hand are used. The hand motions data of grasping are then mapped from the human hand workspace to the two-fingered planer robot hand workspace. Here Barret hand BH282 is used for the demonstration of the mapped motion though it has three fingers. The joint angle positions of Barret hand fingers are calculated using forward and inverse kinematics of the fingers via nonlinear optimization

1 Introduction

Mapping is an important field in robotics. It is used for navigation, localization, path planning in robotics [1]. It is also used widely in telemanipulation and learning by demonstration purposes. For the robotic hand with multiple degrees of freedom, grasp planning is one of the key factors for manipulation. Mapping is one of the principal methods for grasp planning. In human hand/grasp mapping, the hand motion is mapped to the desired robot hand. Mapping is one of the key factors in the telemanipulation of dexterous robotic hands to perform desired jobs. Telemanipulation involves manipulating a robotic hand with versatility and complexity like a human hand by trailing human hand and finger motions.

1.1 Thesis Goals

The objective of this thesis is to map human hand motion to a robotic hand for dexterous telemanipulation. Here the human subject grasps and manipulates an object using thumb and index fingers and the data of the motion is mapped to the robot hand for manipulation. The main goals of the project are given below.

- Transfer the human hand motion from a three-dimensional human hand workspace to a two-dimensional planer space.

- Perform the point-to-point mapping of the fingertips of thumb and index finger to the Barrett Hand fingers.
- Find the joint angles of Barrett Hand fingers for the mapped motions using forward and inverse kinematics of the Barrett Hand.
- Demonstrate the manipulation of Barrett Hand for the mapped motion by using the achieved angles.

1.2 Literature Review

We can divide the human hand motion mapping to the robotic hand into several aspects: Human hand motion capture, mapping to a robotic hand, and manipulation.

First, we need human hand motion data to perform the mapping. There are many ways, the human hand/fingers motion can be captured. But, the most common one is using instrumented gloves. Griffin, Findley, Turner and Cutkosky [2] and Liu and Zhang [3] used CyberGlove® as their motion capture device. There are some benefits and some complexity with the CyberGlove®. The main benefits of this glove are it is portable, lightweight and easy to use. It uses proprietary resistive bend-sensing technology to transform hand motions into real-time digital joint angle data [3]. The main demerit of the glove is a calibration requirement. To capture hand motion with CyberGlove® requires calibration for each user [2]. Compatible kinematic models also required performing motion capture using the glove. Another popular motion capture option is the Vicon Motion Capture System which was used to capture hand motion in this thesis. The Vicon system record the movement of markers placed on human subjects [4]. It captures the position coordinates of each marker placed on the human hand with respect to the reference frame.

There are several methods for human hand mapping. Four of them are widely used, fingertip mapping/point-to-point mapping, joint angle mapping, key point mapping and manipulated object-based mapping [2][5]. Griffin, Findley, Turner and Cutkosky [2] used point-to-point mapping and manipulated object-based mapping methods in their work and compared the results between two methods. Here, in this thesis, fingertip mapping/point-to-point mapping was used as mapping method. Point-to-point mapping is a type of Cartesian space mapping which deals with the geometric relations between the human hand and robot hand workspace [6]. Peer, Einenkel and Buss [7] used point-to-point mapping algorithm to map all the five fingertips' motions of the human hand to a three-fingered robotic gripper. Liu and Zhang [3] also did the mapping of the human hand to a four-fingered robotic hand using the same method.

The mechanism of the human hand is very complex. They can do different kinds of motions, such as grasping, rolling, pinching etc. But, for mapping the human hand to the robot hand, many of the researchers worked only on grasping and rolling. Multi-fingered robotic hands are also complex mechanisms. Many multi-fingered robotic hands were developed by researchers such as DLR hand [8], Barrett hand [9] etc. To avoid complexity, Griffin, Findley, Turner and Cutkosky [2] considered grasping and rolling motions using index and pointer fingers of the human hand and mapped it to a two-fingered planer robot in their work. Liu and Zhang [3] only considered grasping motion but with all five fingers of the human hand in their research and mapped it to a BH4 robotic hand in their work. BH4 is a four-fingered robotic hand with multiple degrees of freedom in each finger.

The works of Griffin, Findley, Turner and Cutkosky [2] were mainly followed in this project. But, the key differences between their work and this work were in the data collection process and mapping method. They used two methods of mapping. Here in this project only the point-to-point mapping method was considered.

1.3 Organization of the thesis

The rest of the thesis is organized as follows: Chapter 2 describes the mathematical background required for this thesis, such as data analysis, mapping algorithm used for this thesis, and forward and inverse kinematics of the Barrett Hand. In chapter 3, motion mapping using the recorded data is shown. Chapter 4 describes the experimental setups required for this thesis. In Chapter 5 and 6, the results, conclusion and future research possibilities on this topic are discussed.

2 Mathematical Background

In this chapter, the mathematical definitions and concepts related to the thesis are reviewed.

2.1 Three-dimensional Space

Cartesian three-dimensional space is a geometric space where three values or parameters are required to define the position [10]. The parameters are x, y, z coordinates. Three-dimensional space is commonly represented by the symbol $\mathbb{R}^3$.

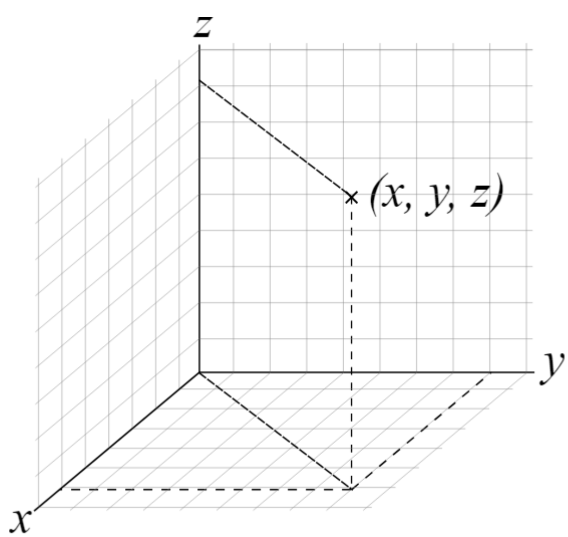

Figure 2.1: Three-dimensional cartesian space

2.2 Kinematics and Rigid Body

"Kinematics is defined as the study of the motion, regardless of the force causing it and caused by it. Motion is a concept that includes position and its derivatives, mainly velocity and acceleration." [11].

The subject that is considered for the study is called a rigid body. "A rigid body is a set of particles such that the distance between them remains fixed. This means that, unlike individual particles, we can define not only location, velocity and acceleration of a particle in the body but also orientation, angular velocity and angular acceleration of the body" [1]. The motion of the rigid body can be defined with translation **d** and rotation [R]. In Figure 2 the motion of a rigid body is shown, where {F} is the fixed frame, **d** the translation and [R] is the rotation.

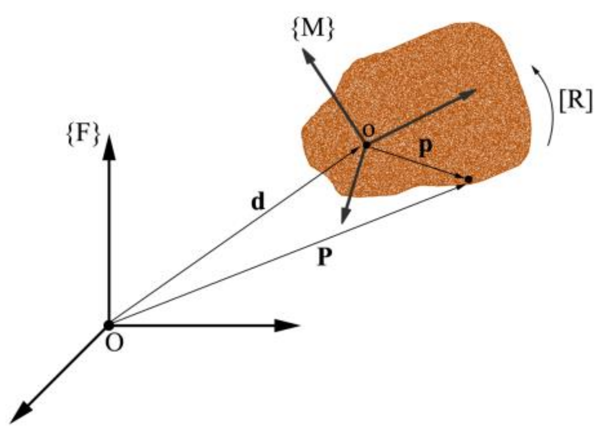

Figure 2.2: Motion of a rigid body

2.3 Translation

In translation motion, all points of the space go the same direction and same amount [11]. In Equation 2.1, a translation example is shown. Figure 2.3(a), shows the translation motion.

$$X = x + t \tag{2.1}$$

Where,

$X = \begin{Bmatrix} X \\ Y \\ Z \end{Bmatrix}$, is the position after translation,

$x = \begin{Bmatrix} x \\ y \\ z \end{Bmatrix}$, is the position before translation,

$t = \begin{Bmatrix} t_x \\ t_y \\ t_z \end{Bmatrix}$, is the translation matrix (direction and magnitude)

2.4 Rotation

In rotation motion, a subspace of points remains fixed and the rest of the points move in a different direction and a different amount according to their location with respect to the fixed points [11]. Rotation is normally denoted with [R]. Equation 2.2 defines a rotation. Figure 2.3(b) shows a rotation motion.

$$X = [R]x \qquad 2.2$$

Where,

$X = \begin{Bmatrix} X \\ Y \\ Z \end{Bmatrix}$, is the position after translation,

$x = \begin{Bmatrix} x \\ y \\ z \end{Bmatrix}$, is the position before translation,

$[R]$ is the rotation matrix.

[R] can be rotation about x or y or z axis or combination of two or more. In Equations 2.3, 2.4, 2.5, rotation matrices about x, y, z axis are shown.

$$[R_x] = \begin{bmatrix} 1 & 0 & 0 \\ 0 & \cos\theta & -\sin\theta \\ 0 & \sin\theta & \cos\theta \end{bmatrix} \qquad 2.3$$

$$[R_y] = \begin{bmatrix} \cos\theta & 0 & \sin\theta \\ 0 & 1 & 0 \\ -\sin\theta & 0 & \cos\theta \end{bmatrix} \qquad 2.4$$

$$[R_z] = \begin{bmatrix} \cos\theta & -\sin\theta & 0 \\ \sin\theta & \cos\theta & 0 \\ 0 & 0 & 1 \end{bmatrix} \qquad 2.5$$

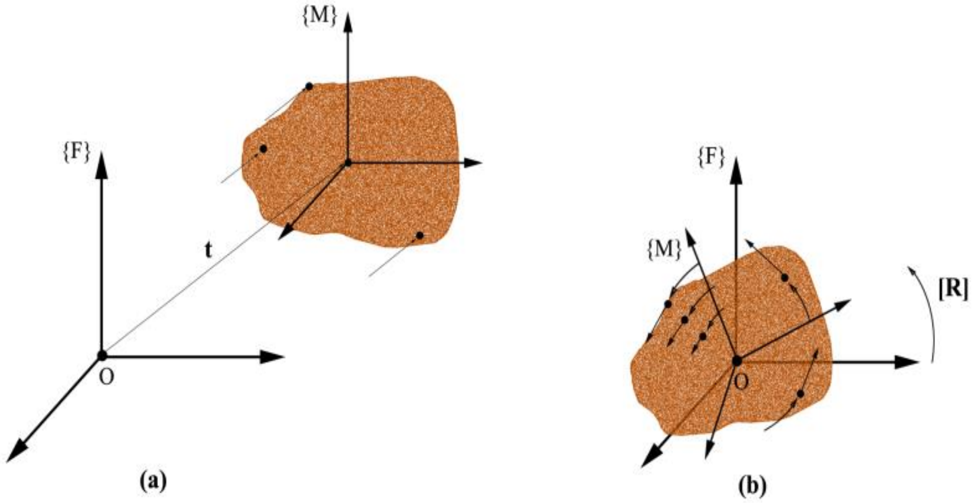

Figure 2.3: (a) translation, (b) rotation

2.5 General Motion

The general motion is the composition of rotation and translation. Equation 2.6 shows the general motion, where 'P' is the final position, 'p' is the initial position, [R] is the rotation and 't' is the translation.

$$P = [R]p + t \tag{2.6}$$

The rotation and translation can be expressed together by a single matrix called the Homogeneous Transformation Matrix. Transformation Matrix can be defined as [T].

$$[T] = \begin{bmatrix} & [R] & & t \\ 0 & 0 & 0 & 1 \end{bmatrix} \tag{2.7}$$

2.6 Composition of Displacements

The transformation matrix of the composition of displacements can be found by matrix multiplication of the transformation matrices of all consecutive displacements. An example of such a transformation matrix is given below.

$$[T] = [T1][T2] = \begin{bmatrix} & [R1] & & t1 \\ 0 & 0 & 0 & 1 \end{bmatrix} \begin{bmatrix} & [R2] & & t2 \\ 0 & 0 & 0 & 1 \end{bmatrix} \qquad 2.8$$

2.7 Least Square Plane Fit and Normal of a Plane

To generate an equation of a plane, three points are required. To find a plane for more than three points, least square fit is necessary. In this section, fit of the plane from a set of n points using the least square method is discussed [12]. A plane can be described by a normal vector $n = [a, b, c]^T$ and a distance 'd', for a point $[x, y, z]^T$ on the plane, the equation of plane can be written as:

$$ax + by + cz + d = 0 \qquad 2.9$$

Considering $c = 1$, Equation 2.9 can be written as follows.

$$ax + by + d = -z \qquad 2.10$$

Then, the equation can be solved for n points in matrix form.

$$\begin{bmatrix} x_0 & y_0 & 1 \\ x_1 & y_1 & 1 \\ & \dots & \\ x_n & y_n & 1 \end{bmatrix} \begin{bmatrix} a \\ b \\ d \end{bmatrix} = \begin{bmatrix} -z_0 \\ -z_1 \\ \dots \\ -z_n \end{bmatrix} \qquad 2.11$$

The transpose of the first matrix from Equation 2.11 is multiplied on both sides of the equation to perform a linear least square.

$$\begin{bmatrix} x_0 & x_1 & \dots & x_n \\ y_0 & y_1 & \dots & y_n \\ 1 & 1 & \dots & 1 \end{bmatrix} \begin{bmatrix} x_0 & y_0 & 1 \\ x_1 & y_1 & 1 \\ & \dots & \\ x_n & y_n & 1 \end{bmatrix} \begin{bmatrix} a \\ b \\ d \end{bmatrix} = \begin{bmatrix} x_0 & x_1 & \dots & x_n \\ y_0 & y_1 & \dots & y_n \\ 1 & 1 & \dots & 1 \end{bmatrix} \begin{bmatrix} -z_0 \\ -z_1 \\ \dots \\ -z_n \end{bmatrix}$$

$$\begin{bmatrix} \Sigma x_i x_i & \Sigma x_i y_i & \Sigma x_i \\ \Sigma y_i x_i & \Sigma y_i y_i & \Sigma y_i \\ \Sigma x_i & \Sigma y_i & N \end{bmatrix} \begin{bmatrix} a \\ b \\ d \end{bmatrix} = - \begin{bmatrix} \Sigma x_i z_i \\ \Sigma y_i z_i \\ \Sigma z_i \end{bmatrix} \qquad 2.12$$

Where N is the number of points, define the x, y, z above in Equation 2.12 to be relative to the centroid (average) of point cloud. Now $\Sigma x = \Sigma y = \Sigma z = 0$ and so Equation 2.12 can be simplified as:

$$\begin{bmatrix} \Sigma x_i x_i & \Sigma x_i y_i & 0 \\ \Sigma y_i x_i & \Sigma y_i y_i & 0 \\ 0 & 0 & N \end{bmatrix} \begin{bmatrix} a \\ b \\ d \end{bmatrix} = - \begin{bmatrix} \Sigma x_i z_i \\ \Sigma y_i z_i \\ 0 \end{bmatrix} \qquad 2.13$$

From the last row ($N \cdot d = 0$) it is found that $d = 0$. This means, the plane always runs through the average of the input points. After getting rid of the dimension:

$$\begin{bmatrix} \Sigma x_i x_i & \Sigma x_i y_i \\ \Sigma y_i x_i & \Sigma y_i y_i \end{bmatrix} \begin{bmatrix} a \\ b \end{bmatrix} = - \begin{bmatrix} \Sigma x_i z_i \\ \Sigma y_i z_i \end{bmatrix} \qquad 2.14$$

From Cramer's rule, the solution for the normal vector is found.

$$D = \sum xx \sum yy - \sum xy \sum xy$$

$$a = (\sum yz \sum xy - \sum xz \sum yy)/D$$

$$b = (\sum xy \sum xz - \sum xx \sum xz)/D$$

So, the normal vector of the plane is $n = [a, b, 1]^T$. Figure 2.4 shows a plane fit from points.

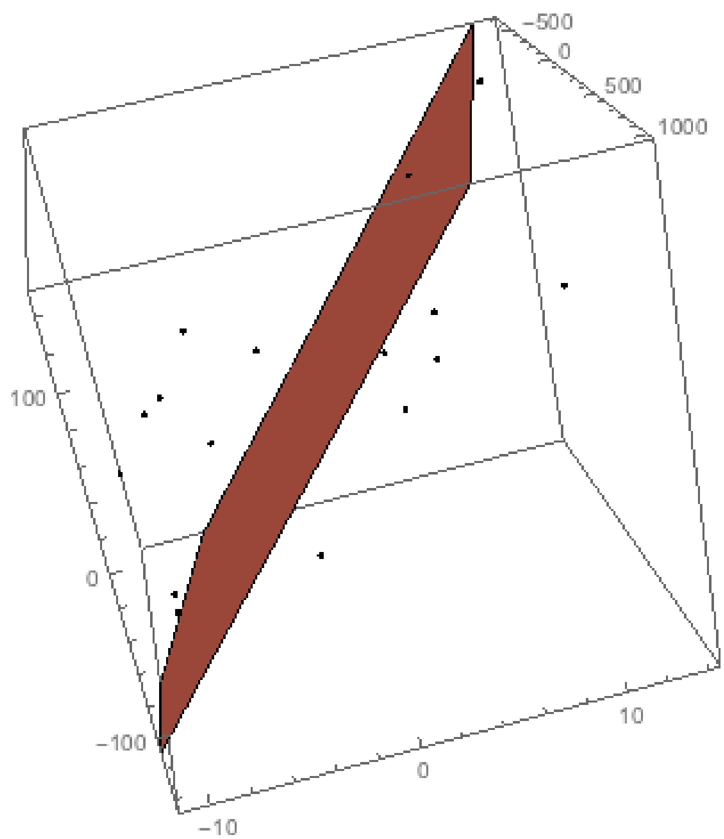

Figure 2.4: Least square fit of a plane from set of n points

2.8 Projection of a Point onto a Plane

A point A (x_0, y_0, z_0) and its projection A' (x, y, z) on the plane P create a line. The direction vector ***s*** of the line coincides with the normal vector ***N*** *(a, b, c)* of the plane P. As the point A' is on the line AA' and the plane P at the same time, the coordinates of the position vector of a variable point of the line can be written in the parametric form:

$x = x_0 + a \cdot t,$

$y = y_0 + b \cdot t$ and

$$z = z_0 + c \cdot t \qquad 2.15$$

If these coordinates are plugged into the equation of the plane P, the value of t will be found. After putting the value of t and the values of a, b, c, on Equation 2.15, the projection point A' (x, y, z) will be found [13].

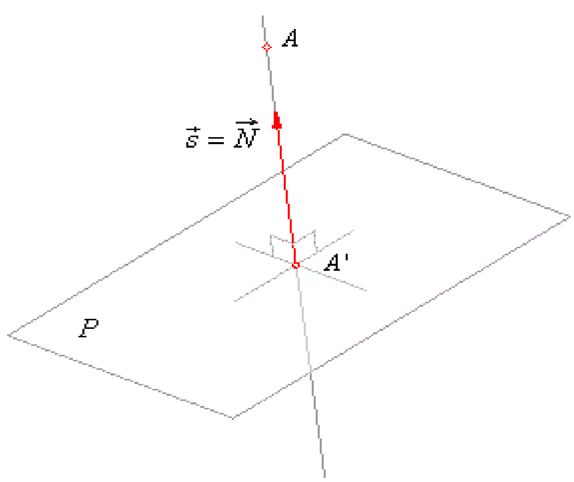

Figure 2.5: Projection of a point onto a plane

2.9 The Denavit-Hartenberg Convention

Denavit-Hartenberg Convention is a methodology of 4x4 homogeneous matrix transformation for inspecting links and joints of robots. In Denavit-Hartenberg Convention, there are four parameters required to define the homogeneous matrix [11] [14]. Those are:

Twist angle $\boldsymbol{\alpha_{i-1,i}}$: Angle between joint axes S_{i-1} and S_i measured about the common normal line $A_{i-1,i}$ [11].

Link length $\boldsymbol{a_{i-1,i}}$: Distance between joint axes S_{i-1} and S_i measured along the common normal line $A_{i-1,i}$ [11].

Joint angle $\boldsymbol{\theta_i}$: Angle between previous common normal line $A_{i-1,i}$ and next common normal line $A_{i,i+1}$, measured about joint axes S_i [11].

Offset $\boldsymbol{d_i}$: Distance between previous common normal line $A_{i-1,i}$ and next common normal line $A_{i,i+1}$, measured along joint axes S_i [11].

Figure 2.6 shows a local transformation of the links of a robot. Table 2.1 shows the required Denavit-Hartenberg (DH) Convention parameter for the Figure 2.1 robot system.

Joint	$\boldsymbol{\alpha_{i-1,i}}$	$\boldsymbol{a_{i-1,i}}$	$\boldsymbol{d_i}$	$\boldsymbol{\theta_i}$
1	0	0	d_1	θ_1
2	α_{12}	a_{12}	d_2	θ_2
3	α_{23}	a_{23}	d_3	θ_3

Table 2.1: Denavit-Hartenberg parameters

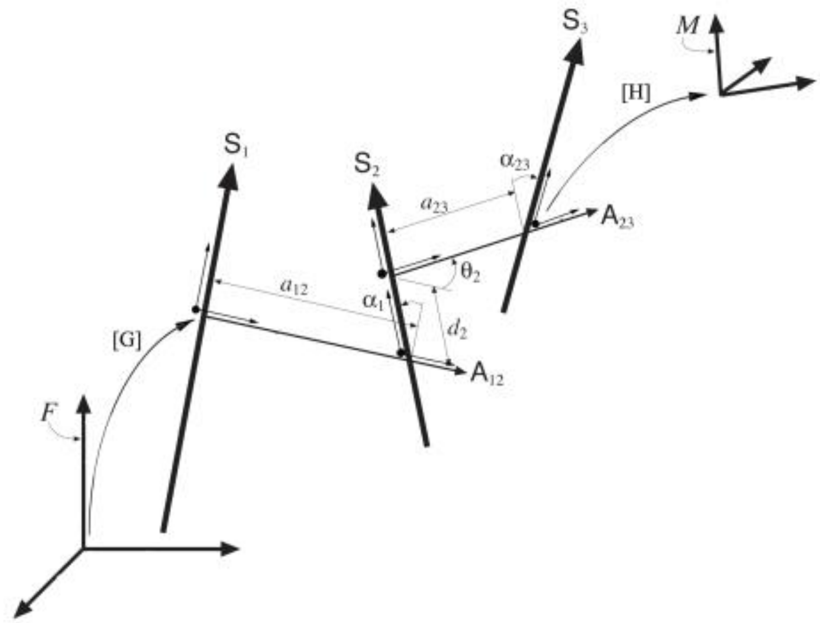

Figure 2.6: Local transformation along the links of a robot

2.10 Forward Kinematics

Forward kinematics deals with the relations between the positions and orientations of the end-effector and the individual joints of the end-effector. From forward kinematics, the position and orientation of the end effector can be found [15].

2.11 Forward kinematics of Barrett Hand

In this thesis, the human hand motion was mapped to the Barrett Hand BH282. The cross-section of the Barrett Hand is shown in Figure 2.7.

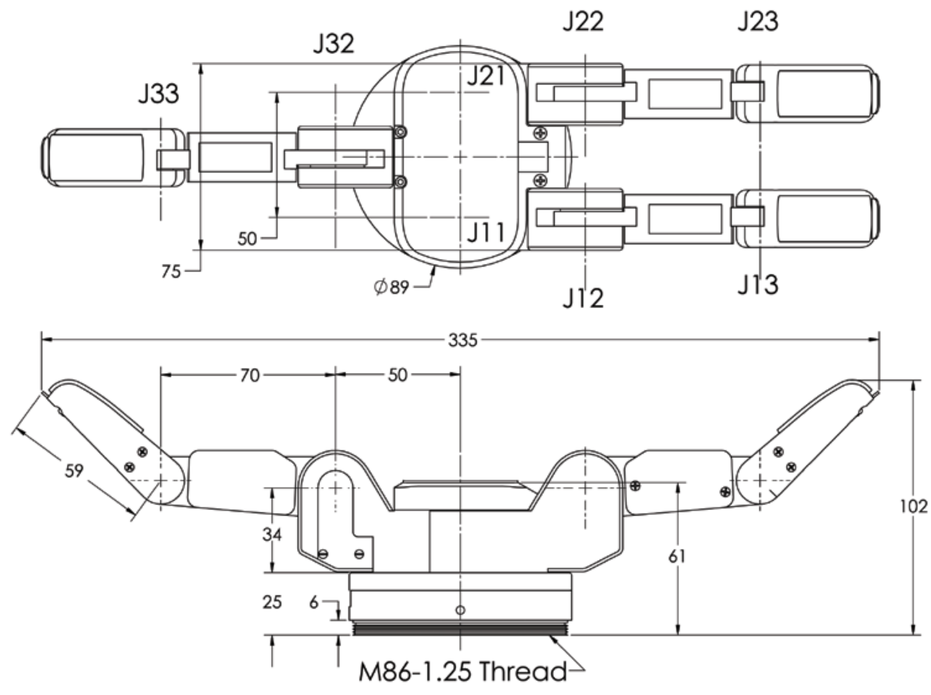

Figure 2.7: Cross-section of Barrett Hand

The forward kinematics of Finger 1 and Finger 3 with respect to the palm are shown below [15] [16]. As Finger 2 has almost the same kinematics of Finger 1, the forward kinematics of Finger 2 isn't shown here. In Table 2.2 the DH parameters, which are applicable for all fingers of BH282, are given.

Parameter	Value
A_1	50mm
A_2	70mm
A_3	50mm
D_0	25mm
D_3	9.5mm
Φ_2	2.46°
Φ_3	50°

Table 2.2: DH parameter values

2.11.1 Forward Kinematics of Finger 1

The DH link parameter values of Finger 1 are given in Table 2.3, and the DH frame of Finger 1 is shown in Figure 2.8

Joint	a_{k-1}	a_{k-1}	d_k	θ_k
1	0	Π	0	Θ_{J41}
2	A_1	$-\pi/2$	0	$\Theta_{J11} + \Phi_2$
3	A_2	0	0	$\Theta_{J12} + \Phi_3$
T	A_3	$-\pi/2$	D_3	0

Table 2.3: DH link parameters of Finger 1

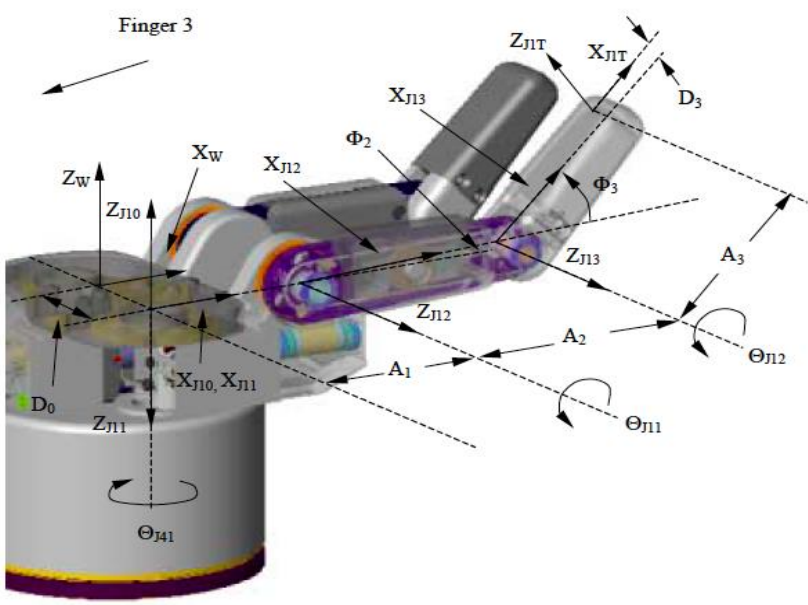

Figure 2.8: DH frame for Finger 1

The final homogeneous transformation matrix of Finger 1 using DH parameters from Table 2.2 and 2.3 is shown below. It gives the final position and orientation of the fingertip of Finger 1 with respect to the palm.

$$ {}_{T}^{W}T = \begin{bmatrix} C_4C_{ab} & S_4 & -C_4S_{ab} & A_3c_4c_{ab} + D_3(-c_4s_{ab}) + A_2c_4c_a + A_1c_4 \\ -S_4C_{ab} & C_4 & S_4S_{ab} & A_3(-s_4c_{ab}) + D_3s_4s_{ab} - A_2s_4s_{ab} - A_2s_4c_a - A_1s_4 - D_0 \\ S_{ab} & 0 & C_{ab} & A_3s_{ab} + D_3c_{ab} + A_2s_a \\ 0 & 0 & 0 & 1 \end{bmatrix} \quad 2.16 $$

Where,

$a = \Theta_{J11} + \Phi_2$

$b = \Theta_{J12} + \Phi_3$

$C_{ab} = cos(a + b)$

$S_{ab} = sin(a + b)$

$C_4 = cos(\Theta_{J41})$

$S_4 = sin(\Theta_{J41})$

2.11.2 Forward Kinematics of Finger 3

As Finger 3 doesn’t have the spread motion along the palm of the hand, the forward kinematics of Finger 3 is little different than Finger 1 and Finger 2. The DH link parameter values of Finger 1 are given in Table 2.3, and the DH frame of Finger 1 is shown in Figure 2.8.

Joint	a_{k-1}	α_{k-1}	d_k	θ_k
1	0	0	0	π
2	A_1	$\pi/2$	0	$\Theta_{J31} + \Phi_2$
3	A_2	0	0	$\Theta_{J32} + \Phi_3$
T	A_3	$-\pi/2$	D_3	0

Table 2.4: DH link parameters of Finger 3

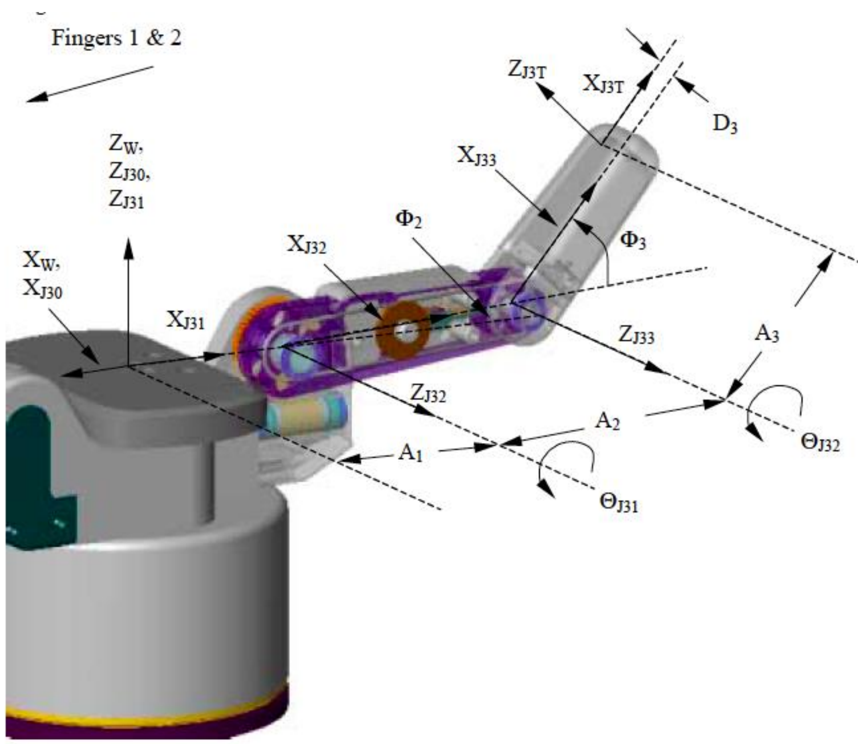

Figure 2.9: DH frame for Finger 3

The final homogeneous transformation matrix of Finger 2 using DH parameters from Table 2.2 and 2.4 is shown below. It gives the final position and orientation of the fingertip of Finger 3 with respect to the palm.

$$ {}^{W}_{T}T = \begin{bmatrix} -C_{ab} & 0 & S_{ab} & -A_3 C_{ab} + D_3 S_{ab} - A_2 C_a - A_1 \\ 0 & 1 & 0 & 0 \\ S_{ab} & 0 & C_{ab} & A_3 S_{ab} + D_3 C_{ab} + A_2 S_a \\ 0 & 0 & 0 & 1 \end{bmatrix} \tag{2.17} $$

Where,

$a = \Theta_{J31} + \Phi_2$

$b = \Theta_{J32} + \Phi_3$

$C_{ab} = cos(a + b)$

$S_{ab} = sin(a + b)$

3 Experimental Setup

Here, the human hand motion was captured using the Vicon Motion Capture System. In this chapter, the motion capture system setup for motion data collection is discussed and the data collection process is discussed.

3.1 Vicon Motion Capture System

The acquisition of hand motion data using the Vicon Motion Capture System was one of the crucial parts of this project. The hand motion tracking system is called Vicon Nexus®. The system consists of 8 infrared cameras and a control box. The cameras are connected to the control box via ethernet cables and the control box is connected to the computer [17]. Figure 3.1 shows the picture of a camera of Vicon Nexus® system.

Figure 3.1: A camera of Vicon Nexus® system

The cameras needed to be placed around the workspace in such a way that the whole workspace could be observed using the cameras. Reflective markers were placed on different parts of the human subject's hand. The cameras tracked the movement of the reflective markers.

Any other reflective objects in the room were removed or covered with black cloths. Otherwise, the system could track the unwanted objects and provide wrong data.

Figure 3.2 shows the general setup of the cameras around the workspace. The version of the software used with the system is Nexus 2.6.1.

Figure 3.2: Vicon motion capture system (camera setup)

3.2 Data Collection

Before starting data collection, the Vicon Nexus® system need to be calibrated. A 'T' shaped wand with reflective markers on it was used for aiming and setting the coordinates plane for the software. The wand was placed in the middle of the workspace and spun around the workspace to calibrate the system.

3.2.1 Marker Placement

Markers were attached to the subject's hand using toupee tape. One important factor about marker placement is that the markers cannot be too close to each other.

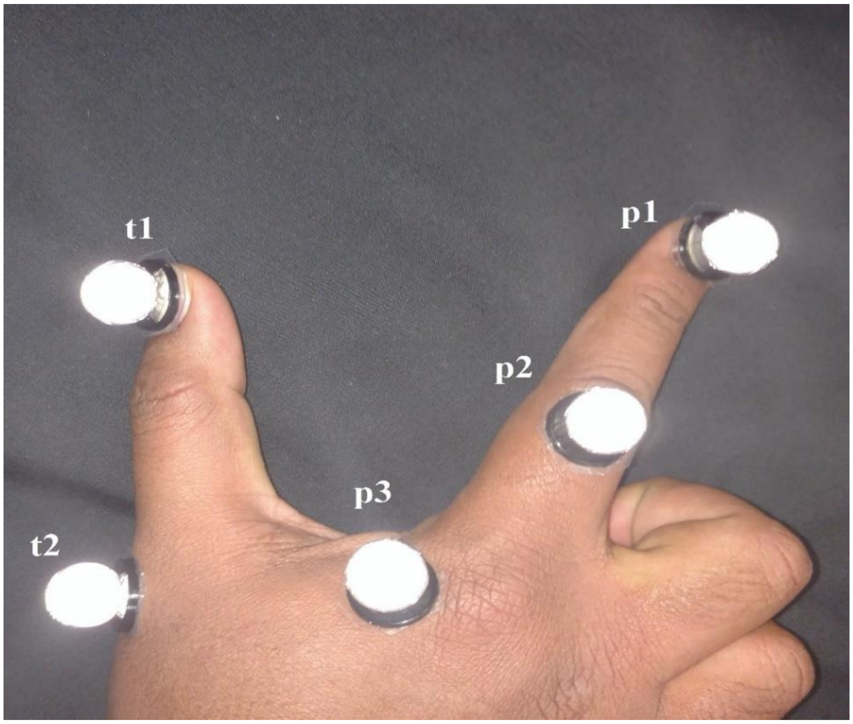

Figure 3.3: Positions of markers on fingers

In this project, only manipulations with two fingers are considered. The fingers are thumbs and index fingers. The markers' position on the hand and fingers were very important for recording fingertip positions, defining different parameters. Here, five markers were used, two on the thumb and three on the index finger. The selected positions of the markers are shown in Figure 3.3. The markers' placement on the hands were:

Marker t_1 on the fingertip of the thumb,

Marker t_2 on proximal interphalangeal joint of the thumb,

Marker p_1 on the fingertip of the index finger,

Marker p_2 on the proximal interphalangeal joint of the index finger,

Marker p_3 on the metacarpophalangeal joint of the index finger.

The subject's hand with markers on it performing a task shown in Figure 3.4.

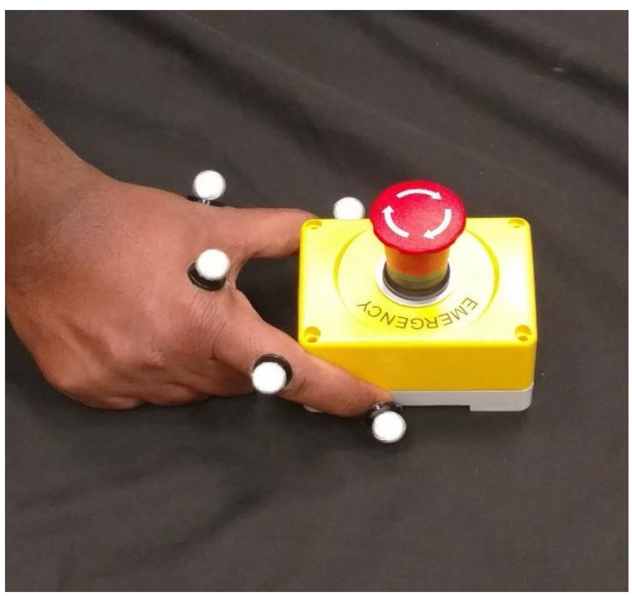

Figure 3.4: Subject performing grasping task

3.2.2 Motion Capture

Different types of motions with the thumb and index fingers were performed for the experiment. Considered motions were grasp and raise an object, grasp and leave an object, and grasp and push an object. Only one subject was used for data acquisition. The Vicon Nexus® software creates a 3D reference frame for the workspace. It records the {x, y, z} coordinates of the positions of the markers with respect to the reference frame. The Vicon Nexus® system captures the motion frame by frame. It took around 10 – 15 seconds to record each motion. Figure 3.5 shows a frame of the motion with the markers in the workspace. There are 373 frames for the grasp and raise motion, 876 frames for the grasp and leave motion, and 641 frames for the grasp and push motion.

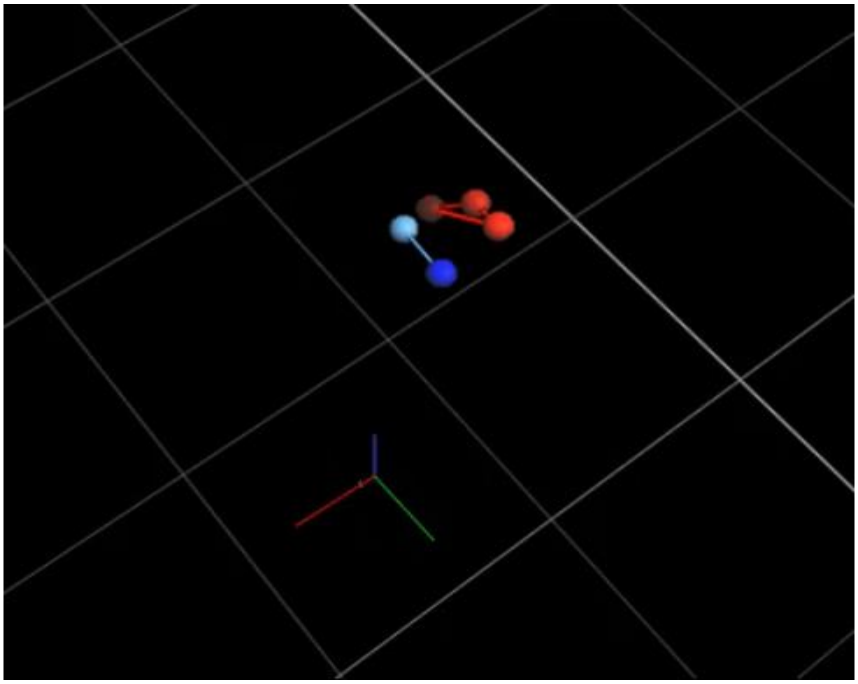

Figure 3.5: Frame of motion

The motion capture data (the {x, y, z} coordinates of the markers, frame after frame) were saved in 'csv' type files. Figure 3.6 shows the snap of the recorded data and Figure 3.7 shows the 3D graph of all the positions of the markers for all the motion considered. In Figure 3.7 the motions of the markers are presented by different colors:

Marker t_1: Red,

Marker t_2: Green,

Marker p_1: Blue,

Marker p2: Black,

Marker p_3: Cyan.

		t1			t2		
Frame	Sub Frame	X	Y	Z	X	Y	Z
		mm	mm	mm	mm	mm	mm
1	0	183.281	649.772	204.064	186.774	708.253	244.315
2	0	181.667	649.047	203.181	185.96	707.591	243.091
3	0	180.681	648.401	202.193	185.262	706.987	241.842
4	0	180.154	647.837	201.078	184.667	706.433	240.501
5	0	179.807	647.277	199.819	184.158	705.855	239.084
6	0	179.468	646.642	198.513	183.708	705.192	237.662
7	0	179.223	645.933	197.188	183.252	704.452	236.214
8	0	179.147	645.15	195.887	182.832	703.647	234.791
9	0	179.335	644.312	194.581	182.442	702.768	233.434
10	0	179.796	643.462	193.304	182.106	701.833	232.182

Figure 3.6: Snap of the motion capture data

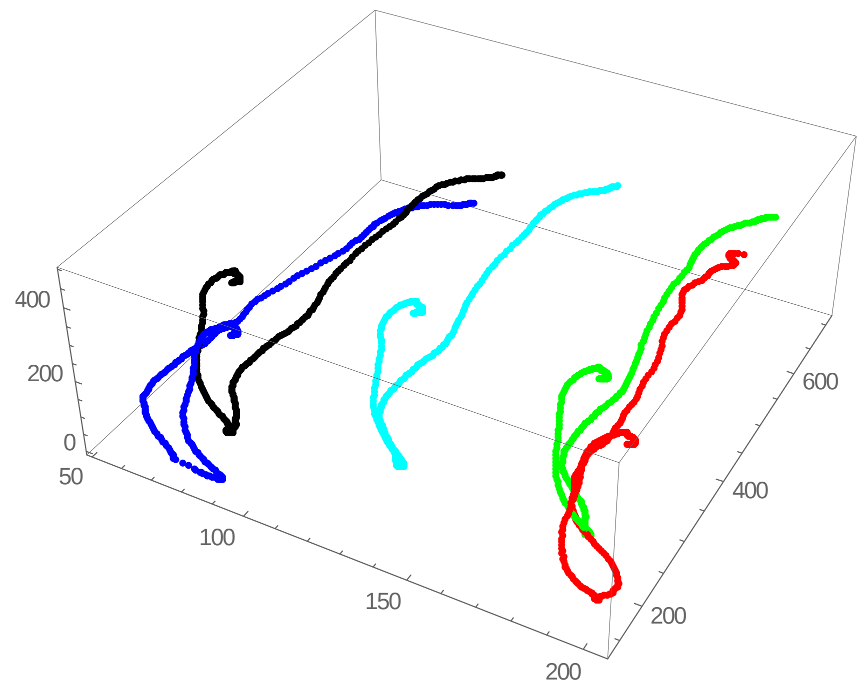

400
200
0
50
100
150
200
200
400
600

(a)

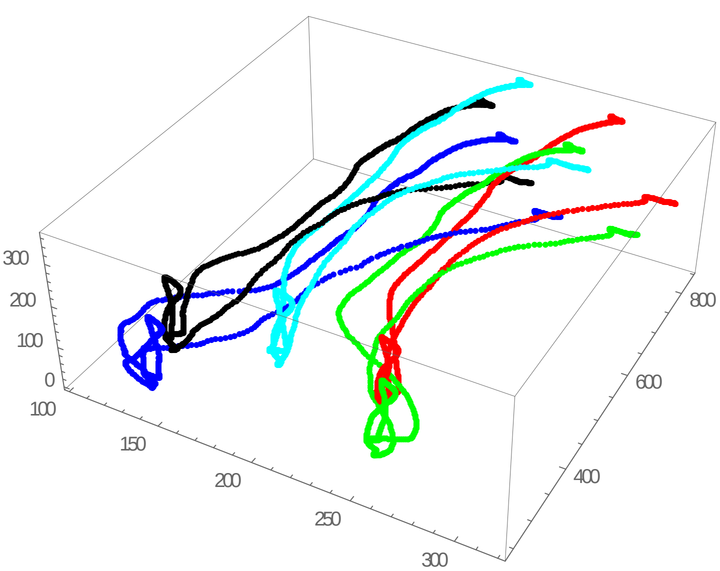

300
200
100
0
100
150
200
250
300
400
600
800

(b)

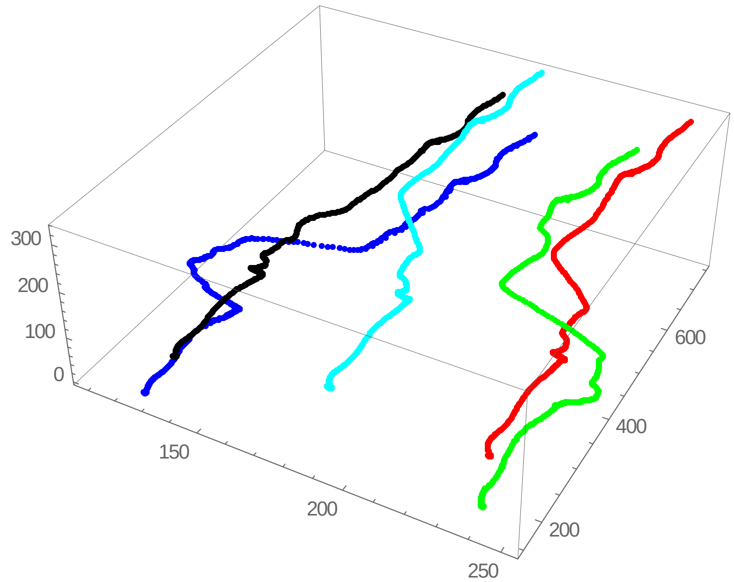

(c)

Figure 3.7: 3D graph of the hand motion for (a) grasp and raise motion, (b) grasp and leave motion, (c) grasp and push motion

4 Mapping

In this project, the human subject grasped and manipulated objects using the thumb and index finger; the resulting hand motion was mapped to a robot hand to perform the same tasks.

Here, the Barrett Hand BH282 was used as the robot hand. The robot hand has different kinematics and workspace than the human hand. So, the mapping from the human hand workspace to the robot hand workspace was necessary. In this project, the human hand workspace was three dimensional and the considered robot motion workspace was planer; therefore, the mapping was needed to transform three-dimensional non-planer motion to the two-dimensional planer motion.

4.1 3D Motions to Planer Motions

The human hand motion considered for the mapping was grasping and raising a stop switch assembly using the thumb and index finger. As it is known, the Vicon Nexus®

system recorded motion frame by frame. For the considered motion, there were 373 frames. The calculations were done for each frame.

Here, each frame has five 3D coordinate positions for five markers. First, planes were defined for each frame. It is known that to define a plane we need only three points. So, getting a plane for all five markers, the least square plane fit method was used here. In the least square method, the best-fit plane can be found for the positions. Mathematica®, an analytical software was used here for the calculations. The positions of the markers for the first frame is given in Table 4.1.

Markers	X coordinate (mm)	Y coordinate (mm)	Z coordinate (mm)
t_1	*183.281*	*649.772*	*204.064*
t_2	*186.774*	*708.253*	*244.315*
p_1	*97.401*	*623.683*	*163.186*
p_2	*102.093*	*660.24*	*213.259*
p_3	*138.609*	*682.194*	*244.336*

Table 4.1: Position of the markers in 1st frame

As an example, the equation of the plane for the first frame from the above positions is given below.

$$-0.02337x + 1.00865y - z = 453.44036$$

The 3D graph of the plane comparing the position of the markers is shown in Figure 4.1. The equations of planes were calculated for each frame i. The normal vectors $T = \{a, b, c\}^i$ for each plane were calculated also.

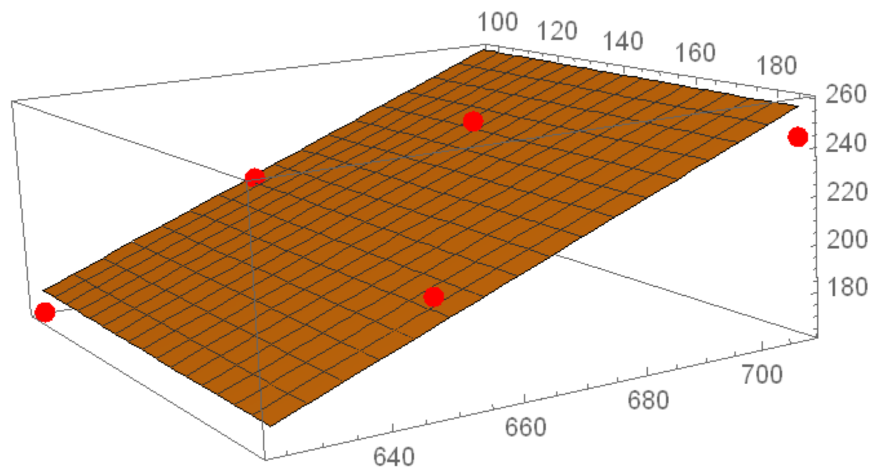

Figure 4.1: Plane for 1st frame of data

After getting the planes for each frame, the next step was to project the positions of the markers onto the plane for each frame. Using the process discussed in chapter 2.8, the projected points for all marker positions for all points were calculated. As an example, projected positions of the markers for the first frame are shown in Figure 3.2. In the Figure, the red points are the original positions of the markers and the blue points are the projected points of the markers. The projected points for each frame were named as $\{Pt_1, Pt_2, Pp_1, Pp_2, Pp_3\}^i$, where i= 1 to 373.

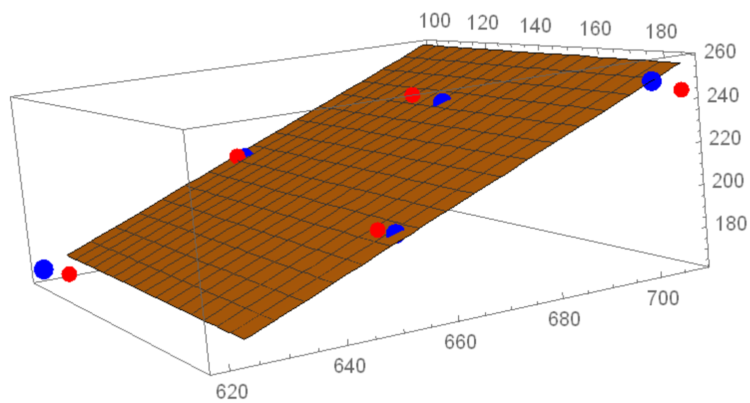

Figure 4.2: Projected points for the 1st frame comparing to the originals

Now the X, Y, Z axis of the local coordinate frames need to be defined for each frame. Point ${Pt_2}^i$ is the center of each local frame. The normalized direction vectors (unit vector) from ${Pt_2}^i$ and ${Pp_2}^i$ are the X axis for all local frames. The unit vectors were calculated as below.

$$X_i\ axis = \frac{{Pp_2}^i - {Pt_2}^i}{\sqrt{\{{Pp_2}^i - {Pt_2}^i\}.\{{Pp_2}^i - {Pt_2}^i\}}}$$

The Y axis of each local frame was calculated by cross multiplying the unit vectors of the X axis with the normal vectors $T$of the corresponding planes and normalizing the results. The Z axis was found by cross multiplying the X axis and Y axis. Here X and Y axes are on the planes and the Z axis is perpendicular to the planes.

After defining the local reference coordinate systems (X, Y, and Z axes) for all time frames, homogeneous transformation matrices were defined for all planes considering ${Pt_2}^i$ as the center of the local frame to transfer all positions of the markers to a single plane.

If the

local $X^i\ axis = \{x_X^i, y_X^i, z_X^i\}$,

local $Y^i\ axis = \{x_Y^i, y_Y^i, z_Y^i\}$,

local $Z^i\ axis = \{x_Z^i, y_Z^i, z_Z^i\}$ and

point ${Pt_2}^i = \{x_{Pt_2}^i, y_{Pt_2}^i, z_{Pt_2}^i\}$

The homogeneous transformation matrices,

$$[T]_i = \begin{bmatrix} X^i & Y^i & Z^i & {Pt_2}^i \\ 0 & 0 & 0 & 1 \end{bmatrix} = \begin{bmatrix} x_X^i & x_Y^i & x_Z^i & x_{Pt_2}^i \\ y_X^i & y_Y^i & y_Z^i & y_{Pt_2}^i \\ z_X^i & z_Y^i & z_Z^i & z_{Pt_2}^i \\ 0 & 0 & 0 & 1 \end{bmatrix}$$

To get the points in the local frame, the inverses of the above homogeneous transformation matrices are multiplied by corresponding points. If the points in the local frame are $\{lt_1, lt_2, lp_1, lp_2, lp_3\}^i$, then

$$\begin{bmatrix} {lt_1}^i \\ 1 \end{bmatrix} = \begin{bmatrix} X^i & Y^i & Z^i & {Pt_2}^i \\ 0 & 0 & 0 & 1 \end{bmatrix}^{-1} \begin{bmatrix} {Pt_1}^i \\ 1 \end{bmatrix}$$

$$\begin{bmatrix} {lt_2}^i \\ 1 \end{bmatrix} = \begin{bmatrix} X^i & Y^i & Z^i & {Pt_2}^i \\ 0 & 0 & 0 & 1 \end{bmatrix}^{-1} \begin{bmatrix} {Pt_2}^i \\ 1 \end{bmatrix}$$

$$\begin{bmatrix} {lp_1}^i \\ 1 \end{bmatrix} = \begin{bmatrix} X^i & Y^i & Z^i & {Pt_2}^i \\ 0 & 0 & 0 & 1 \end{bmatrix}^{-1} \begin{bmatrix} {Pp_1}^i \\ 1 \end{bmatrix}$$

$$\begin{bmatrix} {lp_2}^i \\ 1 \end{bmatrix} = \begin{bmatrix} X^i & Y^i & Z^i & {Pt_2}^i \\ 0 & 0 & 0 & 1 \end{bmatrix}^{-1} \begin{bmatrix} {Pp_2}^i \\ 1 \end{bmatrix}$$

$$\begin{bmatrix} {lp_3}^i \\ 1 \end{bmatrix} = \begin{bmatrix} X^i & Y^i & Z^i & {Pt_2}^i \\ 0 & 0 & 0 & 1 \end{bmatrix}^{-1} \begin{bmatrix} {Pp_3}^i \\ 1 \end{bmatrix}$$

These transformations map all of the points from the three-dimensional human hand workspace to a single planer workspace frame. As all of the points are on a single plane, the Z coordinates of all of points are zero. Figure 3.3 and Figure 3.4 show the points in the planer workspace frame. Here, in Figure 3.3 and Figure 3.4, the corresponding points of

Marker t_1 are Red,

Marker t_2 are Green,

Marker p_1 are Blue,

Marker p2 are Black,

Marker p_3 are Cyan.

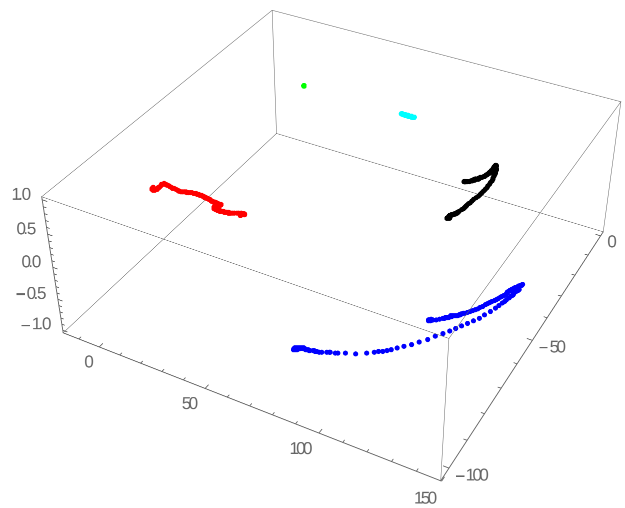

Figure 4.3: Mapped motion of the human hand

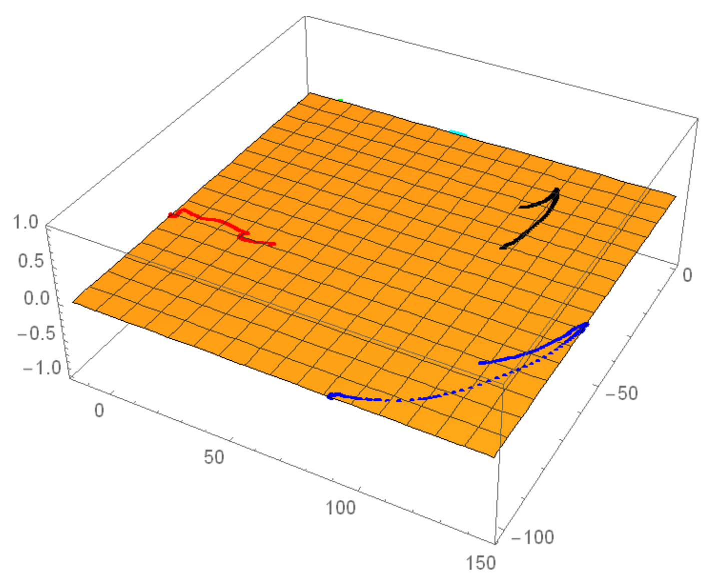

Figure 4.4: Mapped motion of the human hand

4.2 Mapping to Barrett Hand BH282

To do the point-to-point/fingertip mapping of the Barrett Hand BH 282, the forward kinematics of the robot hand is needed. From chapter 2.11.1, the forward kinematics of Finger 1 of the Barrett Hand:

$$ {}^{W}_{T}T^{f1} = \begin{bmatrix} C_4C_{ab} & S_4 & -C_4S_{ab} & A_3C_4C_{ab} + D_3(-C_4S_{ab}) + A_2C_4C_a + A_1C_4 \\ -S_4C_{ab} & C_4 & S_4S_{ab} & A_3(-S_4C_{ab}) + D_3S_4S_{ab} - A_2S_4S_{ab} - A_2S_4C_a - A_1S_4 - D_0 \\ S_{ab} & 0 & C_{ab} & A_3S_{ab} + D_3C_{ab} + A_2S_a \\ 0 & 0 & 0 & 1 \end{bmatrix} \quad 3.1 $$

Where,

$a = \Theta_{J11} + \Phi_2$

$b = \Theta_{J12} + \Phi_3$

$C_{ab} = cos(a + b)$

$S_{ab} = sin(a + b)$

$C_4 = cos(\Theta_{J41})$

$S_4 = sin(\Theta_{J41})$

Only the planer motions of the robot hand were considered. There were no rotations of Finger 1 along the palm of the hand and the finger was considered on the Z_w and X_w plane in Figure 3.5. So, the angle Θ_{J41} representing the rotation was always zero and the offset D_0 was also zero. Therefore,

$C_4 = cos(0) = 1$

$S_4 = sin(0) = 0$

After putting the values of C_4 and S_4, in Equation 3.1 becomes:

$$ {}_{T}^{W}T^{f1} = \begin{bmatrix} C_{ab} & 0 & -S_{ab} & A_3C_{ab} + D_3(-S_{ab}) + A_2C_a + A_1 \\ 0 & 1 & 0 & 0 \\ S_{ab} & 0 & C_{ab} & A_3S_{ab} + D_3C_{ab} + A_2S_a \\ 0 & 0 & 0 & 1 \end{bmatrix} \quad 3.2 $$

The 2nd column and 2nd row can be eliminated from Equation 3.2.

$$ {}_{T}^{W}T^{f1} = \begin{bmatrix} C_{ab} & -S_{ab} & A_3C_{ab} + D_3(-S_{ab}) + A_2C_a + A_1 \\ S_{ab} & C_{ab} & A_3S_{ab} + D_3C_{ab} + A_2S_a \\ 0 & 0 & 1 \end{bmatrix} \quad 3.3 $$

From chapter 2.11., the forward kinematics of Finger 3 of the Barrett Hand:

$$ {}_{T}^{W}T^{f3} = \begin{bmatrix} -C_{ab} & 0 & S_{ab} & -A_3C_{ab} + D_3S_{ab} - A_2C_a - A_1 \\ 0 & 1 & 0 & 0 \\ S_{ab} & 0 & C_{ab} & A_3S_{ab} + D_3C_{ab} + A_2S_a \\ 0 & 0 & 0 & 1 \end{bmatrix} \quad 3.4 $$

Where,

$a = \Theta_{J31} + \Phi_2$

$b = \Theta_{J32} + \Phi_3$

$C_{ab} = cos(a + b)$

$S_{ab} = sin(a + b)$

The 2nd column and 2nd row can be eliminated from Equation 3.4.

$$ {}_{T}^{W}T^{f3} = \begin{bmatrix} -C_{ab} & S_{ab} & -A_3C_{ab} + D_3S_{ab} - A_2C_a - A_1 \\ S_{ab} & C_{ab} & A_3S_{ab} + D_3C_{ab} + A_2S_a \\ 0 & 0 & 1 \end{bmatrix} \tag{3.5} $$

Here, the joints $j11$ and $j12$ of Finger 1 are linked together and actuated by a single actuator. The joint angle (Θ_{J12}) for joint $j12$ moves 1/3 of the movement of the joint angle (Θ_{J11}) for joint $j11$. It is the same for the Finger 3. The joint angle (Θ_{J32}) for joint $j32$ moves 1/3 of the movement of the joint angle (Θ_{J31}) for joint $j31$. Therefore,

$\Theta_{J12} = \frac{\Theta_{J11}}{3}$ and $\Theta_{J32} = \frac{\Theta_{J31}}{3}$.

Putting all the values in Equations 3.3 and 3.5 from above and from Table 2.2:

$$ {}_{T}^{W}T^{f1} = \begin{bmatrix} \mathrm{Cos}[0.9156 + \frac{4\theta j11}{3}] & -\mathrm{Sin}[0.9156 + \frac{4\theta j11}{3}] & 50 + 70\mathrm{Cos}[0.0429 + \theta j11] + 50\mathrm{Cos}[0.9156 + \frac{4\theta j11}{3}] - 9.5\mathrm{Sin}[0.9156 + \frac{4\theta j11}{3}] \\ \mathrm{Sin}[0.9156 + \frac{4\theta j11}{3}] & \mathrm{Cos}[0.9156 + \frac{4\theta j11}{3}] & 9.5\mathrm{Cos}[0.9156 + \frac{4\theta j11}{3}] + 70\mathrm{Sin}[0.0429 + \theta j11] + 50\mathrm{Sin}[0.9156 + \frac{4\theta j11}{3}] \\ 0 & 0 & 1 \end{bmatrix} \tag{3.6} $$

$$ {}_{T}^{W}T^{f3} = \begin{bmatrix} -\mathrm{Cos}[0.9156 + \frac{4\theta j31}{3}] & \mathrm{Sin}[0.9156 + \frac{4\theta j31}{3}] & -50 - 70\mathrm{Cos}[0.0429 + \theta j31] - 50\mathrm{Cos}[0.9156 + \frac{4\theta j31}{3}] + 9.5\mathrm{Sin}[0.9156 + \frac{4\theta j31}{3}] \\ \mathrm{Sin}[0.9156 + \frac{4\theta j31}{3}] & \mathrm{Cos}[0.9156 + \frac{4\theta j31}{3}] & 9.5\mathrm{Cos}[0.9156 + \frac{4\theta j31}{3}] + 70\mathrm{Sin}[0.0429 + \theta j31] + 50\mathrm{Sin}[0.9156 + \frac{4\theta j31}{3}] \\ 0 & 0 & 1 \end{bmatrix} \tag{3.7} $$

In point-to-point/fingertip mapping, the motions of the fingertips of the human hand, fingers are mapped to the end-effector of the robot hand fingers. Here the fingertip positions of the thumb and index fingers in the human hand workspace are t_1 and p_1

respectively; and the respective fingertip positions of t_1 and p_1 in the planer frame are lt_1 and lp_1. lt_1 positions were mapped to the Finger 3 of the Barrett Hand and lp_1 positions were mapped to the Finger 1 of the Barrett Hand. In Figure 4.5, the motion of lt_1 and lp_1 are shown in 2D, where blue represents the motion of lt_1(thumb) and black represents the motion of lp_1(index finger). Considering coordinates of lt_1 and lp_1 are:

$$lt_1 = \{x_{lt1}, y_{lt1}, 0\}^i,$$

$$lp_1 = \left\{x_{lp1}, y_{lp1}, 0\right\}^i.$$

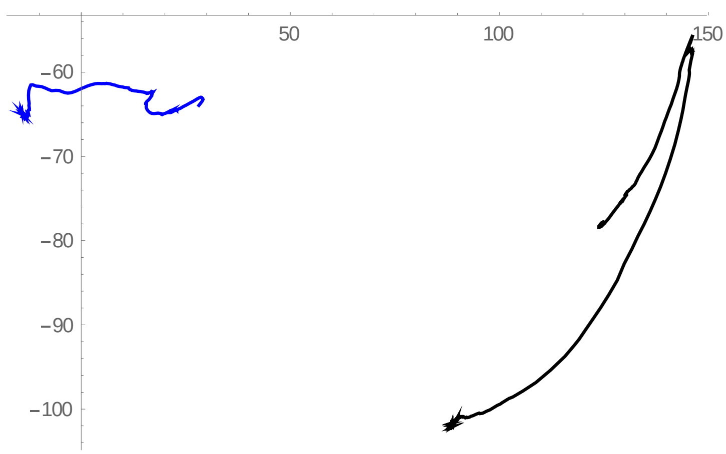

Figure 4.5: Motions of lt_1 and lp_1

To map the lt_1 and lp_1 positions to the end-effectors of Finger 1 and 3 of the Barrett Hand, another transformation matrix (Equation 3.8) from planer frame to robot hand frame is introduced below.

$$ {}_{p}^{r}T = \begin{bmatrix} \mathrm{Cos}[\theta] & -\mathrm{Sin}[\theta] & 0 & \mathrm{xo} \\ \mathrm{Sin}[\theta] & \mathrm{Cos}[\theta] & 0 & \mathrm{yo} \\ 0 & 0 & 1 & 0 \\ 0 & 0 & 0 & 1 \end{bmatrix} \qquad 3.8 $$

In Equation 3.8, θ is the rotation motion and $\{xo, yo, 0\}$ is the translation motion of the frame to robot workspace. Column 3 and row 3 can be eliminated. So, the Equation 3.8 become:

$$ {}_{p}^{r}T = \begin{bmatrix} \mathrm{Cos}[\theta] & -\mathrm{Sin}[\theta] & \mathrm{xo} \\ \mathrm{Sin}[\theta] & \mathrm{Cos}[\theta] & \mathrm{yo} \\ 0 & 0 & 1 \end{bmatrix} \qquad 3.9 $$

After multiplying ${}_{p}^{r}T$ with ${}_{T}^{W}T^{f1}$ and ${}_{T}^{W}T^{f1}$ separately, we get:

$$ \left[{}_{p}^{r}T\right]\left[{}_{T}^{W}T^{f1}\right] = \begin{bmatrix} M11 & M12 & M13 \\ M21 & M22 & M23 \\ 0 & 0 & 1 \end{bmatrix} \qquad 3.10 $$

$$ \left[{}_{p}^{r}T\right]\left[{}_{T}^{W}T^{f3}\right] = \begin{bmatrix} N11 & N12 & N13 \\ N21 & N22 & N23 \\ 0 & 0 & 1 \end{bmatrix} \qquad 3.11 $$

Where,

$M13 = \mathrm{xo} + \mathrm{Cos}[\theta](50 + 70\mathrm{Cos}[0.0429 + \theta\mathrm{j}11] + 50\mathrm{Cos}[0.9156 + \frac{4\theta\mathrm{j}11}{3}] -$
$9.5\mathrm{Sin}[0.9156 + \frac{4\theta\mathrm{j}11}{3}]) - \mathrm{Sin}[\theta](9.5\mathrm{Cos}[0.9156 + \frac{4\theta\mathrm{j}11}{3}] + 70\mathrm{Sin}[0.0429 + \theta\mathrm{j}11] +$
$50\mathrm{Sin}[0.9156 + \frac{4\theta\mathrm{j}11}{3}])$,

$M23 = \text{yo} + \text{Sin}[\theta](50 + 70\text{Cos}[0.0429 + \theta\text{j}11] + 50\text{Cos}[0.9156 + \frac{4\theta\text{j}11}{3}] - 9.5\text{Sin}[0.9156 + \frac{4\theta\text{j}11}{3}]) + \text{Cos}[\theta](9.5\text{Cos}[0.9156 + \frac{4\theta\text{j}11}{3}] + 70\text{Sin}[0.0429 + \theta\text{j}11] + 50\text{Sin}[0.9156 + \frac{4\theta\text{j}11}{3}])$,

And

$N13 = \text{xo} + \text{Cos}[\theta](-50 - 70\text{Cos}[0.0429 + \theta\text{j}31] - 50\text{Cos}[0.9156 + \frac{4\theta\text{j}31}{3}] + 9.5\text{Sin}[0.9156 + \frac{4\theta\text{j}31}{3}]) - \text{Sin}[\theta](9.5\text{Cos}[0.9156 + \frac{4\theta\text{j}31}{3}] + 70\text{Sin}[0.0429 + \theta\text{j}31] + 50\text{Sin}[0.9156 + \frac{4\theta\text{j}31}{3}])$,

$N23 = \text{yo} + \text{Sin}[\theta](-50 - 70\text{Cos}[0.0429 + \theta\text{j}31] - 50\text{Cos}[0.9156 + \frac{4\theta\text{j}31}{3}] + 9.5\text{Sin}[0.9156 + \frac{4\theta\text{j}31}{3}]) + \text{Cos}[\theta](9.5\text{Cos}[0.9156 + \frac{4\theta\text{j}31}{3}] + 70\text{Sin}[0.0429 + \theta\text{j}31] + 50\text{Sin}[0.9156 + \frac{4\theta\text{j}31}{3}])$,

As, $M13$ and $M23$ are representing the end-effector's X and Y coordinate positions of Finger 1 and $N13$ and $N23$ are representing the end-effectors' X and Y coordinate positions of Finger 2, It is considered that the

$$M13 = x_{lp1}^{i},\ M23 = y_{lp1}^{i} \tag{3.12}$$

$$N13 = x_{lt1}^{i},\ N23 = y_{lt1}^{i} \tag{3.13}$$

Where $i = 1\ to\ 373$

Initially, 8 values are considered (sequentially 45 values apart from one another) for each of $x_{lp1}^{i}, y_{lp1}^{i}, x_{lt1}^{i}, y_{lt1}^{i}$ coordinates and Equations 3.12 and 3.13 are minimized for the values to find out xo, yo, θ using the Levenberg–Marquardt algorithm with the help of MATLAB® optimization tool as the system of equations are nonlinear overdetermined system. The values found for xo, yo, θ are given in Table 4.2. 8 values of joint angle θj11 and 8 values of θj31 are also found. The values of $xo, yo, \theta$are then plugged to the $M12$, $M23$, $M12$ and $M23$.

xo	yo	θ
98.5933	-154.7555	-0.0735. 8

Table 4.2: Values of xo, yo and θ

All the values of joint angles θj11 and θj31 are found by solving Equations 3.12 and 3.13 for $i = 1\ to\ 373$ using the Levenberg–Marquardt algorithm in MATLAB®.

5 Results

The values of joint angles θj11 and θj31 of the Barrett Hand that are found by mapping human hand motion, are tested using the Physical Barrett Hand BH282.

The mapping method used here is not perfect. The robot hand cannot perform the expected motion by this mapping method. Figure 5.1 shows the comparison between the achieved robot fingertip positions of the finger1 and Finger 3 of the Barret Hand and the expected positions. Here red and green points are the achieved trajectories of Finger 3 and Finger 1 of Barrett Hand respectively. Blue and black points are representing the trajectories that are attempted to be reached by Finger 3 and Finger 1 respectively.

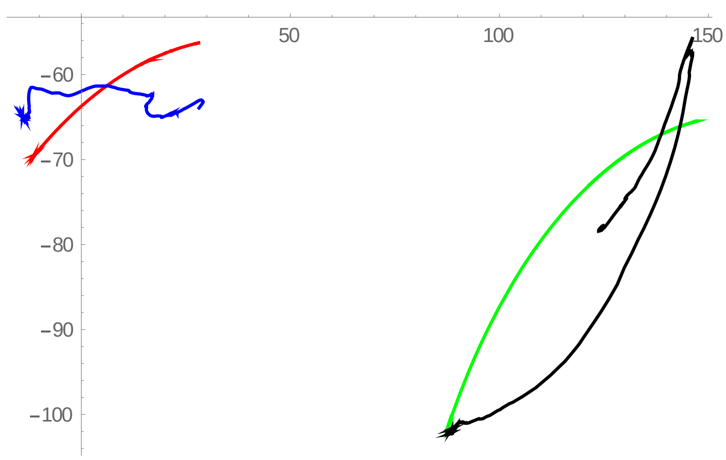

Figure 5.1: Expected and achieved trajectories of the motion of the robot fingers

From Figure 5.1, it is seen that the end-effector positions of Finger 3 are far away from the attempted positions at the beginning and the end of the motion and closer at the middle of the motion. The end-effector positions of Finger 1 are far away from the attempted positions at the middle of the motion and nearer during the start and the end. Figure 5.2, shows the fingertip positions and joint angles of the Finger 1 and Finger 3 of the Barrett Hand for 8 positions.

One suspected reason behind the errors is that the attempted points are outside of the robot hand fingers' workspace. Another reason could be the Levenberg–Marquardt algorithm. Probably, the solutions that are found for xo, yo, θ using the Levenberg–Marquardt algorithm are not in the global minimization point.

By modifying the mapping parameters, using a different method to solve a nonlinear overdetermined system, a better result could be achieved.

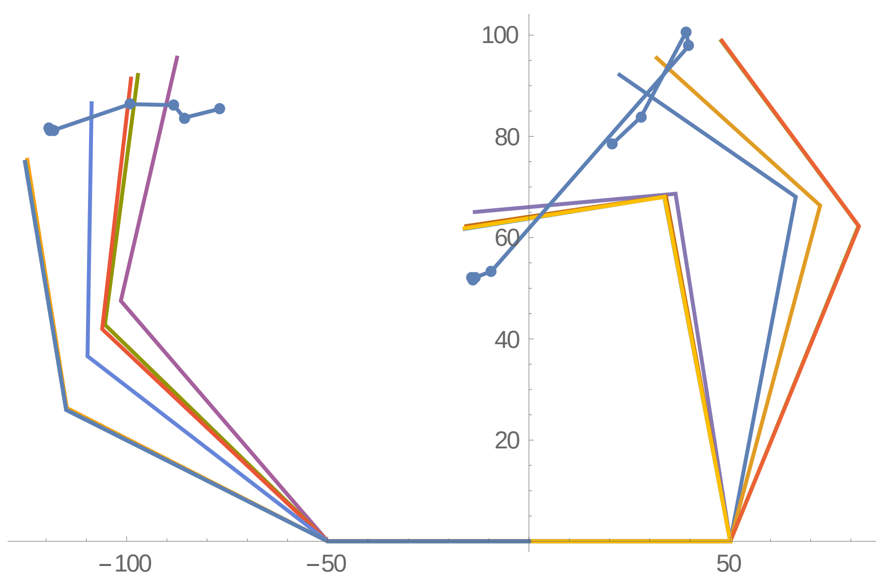

Figure 5.2: Finger 1 and 3 positions and joint angles for 8 positions

6 Conclusion

This project presents the mapping of human hand motions to the robot hand. Human hand motions were captured using the Vicon motion capture system. Initially, the human hand motions were converted to planer motion. Then using the fingertip mapping method, the motions were mapped to the Barret Hand, a robot hand developed by Barrett Technology, LLC. The joint angles of the Barrett Hand fingers were calculated for the motions.

In previous related works, researchers mostly used instrumented gloves to record the motion of the human hand. Use of the Vicon motion capture system for capturing human hand motion for mapping is new. So, scopes of improvements are available here.

There are some issues with the mapping parameters which are discussed in the previous chapter. In the future, more precise mapping parameters can be used to achieve better results. Two or more mapping methods can be used for the mapping and results can be compared to the methods. Some other types of human hand motion, such as rolling, can be considered for mapping.

References

[1] Siciliano, B., & Khatib, O. (2016). *Springer handbook of robotics*. Berlin: Springer.

[2] Griffin, W. B., Findley, R. P., Turner, M. L., Cutkosky, M. R. (2000). Calibration and Mapping of a Human Hand for Dexterous Telemanipulation. *ASME IMECE 2000 Symposium on Haptic Interfaces for Virtual Environments and Teleoperator Systems*, pp. 1–8.

[3] Liu, J., & Zhang, Y. (2007). Mapping human hand motion to dexterous robotic hand. *2007 IEEE International Conference on Robotics and Biomimetics (ROBIO).* doi:10.1109/robio.2007.4522270

[4] Heidari, O., Roylance, J. O., Perez-Gracia, A., & Kendall, E. (2016). Quantification of Upper-Body Synergies: A Case Comparison for Stroke and Non-Stroke Victims. *Volume 5A: 40th Mechanisms and Robotics Conference*. doi:10.1115/detc2016-59314

[5] Hu, H., Gao, X., Li, J., Wang, J., & Liu, H. (2004). Calibrating human hand for teleoperating the HIT/DLR hand. *IEEE International Conference on Robotics and Automation, 2004. Proceedings. ICRA 04. 2004*. doi:10.1109/robot.2004.1302438

[6] Gioioso, G., Salvietti, G., Malvezzi, M., & Prattichizzo, D. (2012). An Object-Based Approach to Map Human Hand Synergies onto Robotic Hands with Dissimilar Kinematics. *Robotics: Science and Systems VIII*. doi:10.15607/rss.2012.viii.013

[7] Peer, A., Einenkel, S., & Buss, M. (2008). Multi-fingered telemanipulation - mapping of a human hand to a three finger gripper. *RO-MAN 2008 - The 17th IEEE International*

Symposium on Robot and Human Interactive Communication.
doi:10.1109/roman.2008.4600710

[8] Liu, Y. (2009). Five-finger Dextrous Robot Hand DLR/HIT Hand II. *Journal of Mechanical Engineering, 45*(11), 10. doi:10.3901/jme.2009.11.010

[9] BarrettHand™ / Overview. (n.d.). Retrieved December 29, 2017, from http://www.barrett.com/products-hand.htm

[10] Three-dimensional space. (2017, December 28). Retrieved December 30, 2017, from https://en.wikipedia.org/wiki/Three-dimensional_space

[11] Gracia, A. P. (n.d.). *Kinematics of Robots*

[12] Fitting a plane to many points in 3D. (2015, March 04). Retrieved December 31, 2017, from http://www.ilikebigbits.com/blog/2015/3/2/plane-from-points

[13] Projection of a point onto a plane (n.d.). Retrieved December 31, 2017, from http://www.nabla.hr/CG-LinesPlanesIn3DB5.htm#Projection of a point onto a plane

[14] SPONG, M. W., Hutchinson, S., Vidyasagar, M., (2012). *ROBOT MODELING AND CONTROL*. JOHN WILEY & Sons.

[15] Sharif, S. M. (n.d.). *Position control strategies for the Barrett Hand* (Unpublished master's thesis).

[16] BarrettHand BH8-280/282 Kinematics, joint ranges, conversion factors. (n.d.). Retrieved December 31, 2017, from
http://support.barrett.com/wiki/Hand/280/KinematicsJointRangesConversionFactors.

[17] Roylance, J. O. (n.d.). *The quantification of upper body synergies: a case comparison for stroke and non-stroke victims* (Unpublished master's thesis).